

Monitoring Dams and Reservoir Slopes with Interferometric SAR

Malte Vöge*), Yngvar Larsen**), Regula Frauenfelder*)

*) NGI, Norway

**) Norut, Norway

1 Introduction

Monitoring of dams and their reservoirs is important to ensure the safety of adjacent and nearby areas, especially in view of the increasing age of many of these structures. In order to ensure early recognition of problem areas at the dam itself and/or at the slopes around the reservoir, frequent displacement measurements are necessary. Traditionally, displacements at the dam are measured by geodetic measurements. Such measurements are time consuming and, thus, expensive. Monitoring reservoir slopes in this manner is not feasible due to the large area to be covered.

The use of satellite based interferometric synthetic aperture radar (InSAR) can provide displacement measurements with a precision in the millimeter range. There are various advantages over ground-based methods: a) satellite images provide coverage of large areas, b) modern SAR satellites provide high spatial resolution, c) data can be acquired frequently and at moderate costs and d) satellite based measurements provide up to 19 year long records of historic measurements

Here, we present results of an InSAR study on displacements at the Svartevann dam in south-west Norway.

2 Target Area

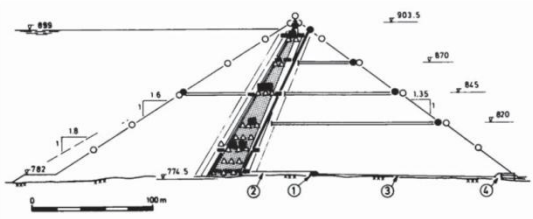
Svartevann dam is an earth-rock-filled dam constructed between 1973 and 1976. It is situated at an elevation of 900 m above normal sea level and holds the uppermost and largest reservoir of the Sira-Kvina Hydroelectrical Scheme in Western Norway. The dam has a height of 129 m and a crest length of 400 m and a total volume of 4.7 hm³. The dam has a storage capacity of 1400hm³ and with a total water head potential of 900m it has a

capacity of 1400 MW generated by a series of power stations. Figure 1 shows an aerial photograph of the dam under construction.

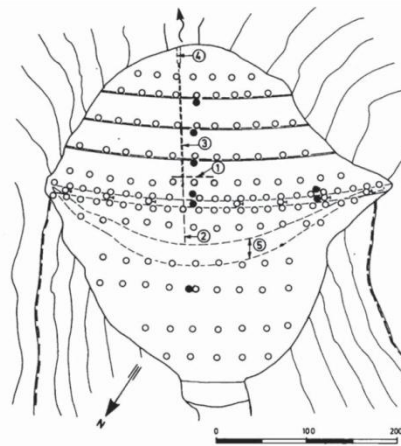


Figure 1: Aerial photograph of the Svartevann dam during construction (courtesy entrepreneur F.Selmer / Høyer-Ellefsen)

The dam is founded entirely on solid rock. Loose overburden was removed before construction of the dam. The structure of the dam consists of 6 zones. The core of the dam is made of the moraine till. It is surrounded by two filter zones of natural sandy gravel and tunnel spoil or quarry run rock (<0.3 m rock diameter). The following supporting rockfill zone consists of granite gneiss. The slopes and the crest are covered by layer of large stones (>0.75 t) to protect the underlying structure. Figure 2a shows a cross-section of the dam structure. For more details on the design and construction of Svartevann dam see [Kjærnsli et al, 1982].



- Reference plate
- Surface monuments
- △ Pore pressure piezometer
- Earth pressure cells, single and rosette
- Casing for measurement of displacement
- ≡ Extensometers



- ① Seepage barrier
- ② Concrete wall
- ③ Pipelines
- ④ Instrument house
- ⑤ Core

Figure 2: Design of Svartevann dam and overview of instrumentation for displacement monitoring (figures taken from [DiBiagio et al, 1982]).

In order to monitor surface displacements a network of 141 monuments has been installed. 42 monuments were installed on the upstream slope, 47 along the crest and 52 on the downstream slope. In addition, 8 reference plates have been installed along the crest (see Figure 2b). Horizontal and vertical movements of the reference monuments are determined by geodetic observations from 6 geodetic stations [DiBiagio et al, 1982].

Figure 3 shows the displacements derived from two geodetic surveys just after completion of the dam and 4 years after completion of the dam. The displacements are shown as contour plots for the three orthogonal components of displacement, i.e., radial and tangential to the dam axis and the vertical direction (settlement). The symmetry of the contours reflects the shape of the valley underneath the dam. Although the displacements are relatively large, the displacement patterns are as expected shortly after completion of the dam.

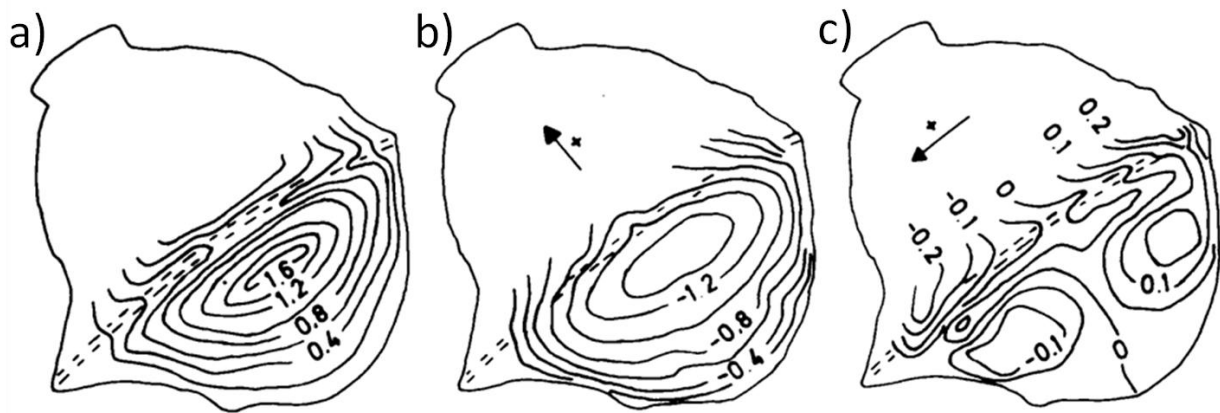


Figure 3: Displacements in meters within the first 4 years after completion; a) settlement; b) displacement radial to dam axis; c) displacement tangential to dam axis (figures taken from [DiBiagio et al, 1982]).

3 Methodology

SAR interferometry can be used to measure ground displacements at very high accuracy. The most basic approach is the Differential InSAR technique, see e.g. [Massonet and Feigl, 1998]. Here, the interferogram of a single image pair is calculated and the deformation derived from the resulting phase difference. However, deformation is not the only source for phase differences. Due to the incidence angle of the radar beam (e.g. 23° for ERS1/2) and the fact that the satellite will not have the exact same position for the two acquisitions, topography can have a strong impact on the interferometric phase. The larger the spatial distance between acquisitions (spatial baseline), the larger the topography induced interferometric phase. Furthermore, differences in the atmosphere (temperature, water vapor) can contribute to the interferometric phase as well as inaccuracies in the orbit information of the satellite. Using a digital elevation model (DEM) and precise orbits (that are available for almost all modern satellites) these phase contributions can be compensated for. Without additional metrological data, this is not possible for the atmospheric phase.

Another effect that plays an important role in SAR interferometry is the temporal decorrelation. The longer time span between acquisitions (temporal baseline), the more changes will occur on the earth's surface, e.g. due to vegetation or constructions. This will

cause decorrelation of the interferometric phase. Therefore, single pair interferometry is best suited for sudden displacements (e.g. an earthquake), that can be measured using two SAR scenes just before and after the displacement event. Slow movements in the range of a few mm/year cannot be measured, since either the temporal baseline is too long to achieve good coherence, or the temporal baseline is so short, that the amount of displacement between acquisitions is too small to be detectable.

This dilemma led to the development of InSAR processing techniques for time-series of SAR scenes. The Permanent Scatterer technique (PS-InSAR) was introduced by [Ferretti et al., 2000]. Here, interferograms are calculated for each of a larger stack of scenes (>20) with respect to one common master. From these interferograms PS-InSAR identifies point-like reflectors that are characterized by very stable amplitude of the backscatter. Filter techniques can then be used to compensate for topographic and atmospheric phases due to their different spatial and temporal characteristics. While the resolution of the original SAR data is preserved, a disadvantage of the technique is the often low density of permanent scatterers, especially in natural terrains with a limited amount of point-like reflectors.

A technique better suited for natural terrains, and also for larger structures like dams, is the Small Baseline Subset (SBAS) algorithm [Berardino et al, 2002]. Here, interferograms are calculated for all possible combinations of an image stack that are below certain limits for temporal and spacial baselines. This reduces the effect of temporal and spacial decorrelation. The vector $\delta\Phi$ of differential phase images and matrix \mathbf{B} that contain the interferogram connectivity and the temporal separation build a linear equation system that results in the ground velocity time-series \mathbf{v} :

$$\mathbf{B} \mathbf{v} = \delta\Phi$$

If the set of interferograms is fully connected, \mathbf{B} is well or over determined and the equation can be solved by least-squares methods. However, in practice the availability of a long time-series with dense temporal sampling is often not given. For satellites like ERS1/2 SAR time-series often have gaps with a large temporal baseline. In this case the equation system can be solved by singular value decomposition (SVD) with a minimum norm constraint on the resulting velocity time-series. For further information on the SBAS algorithm refer to [Berardino et al,2002].

For the presented work we chose to apply the SBAS algorithm. The area around the Svartevann reservoir is not populated and also the dam it-self is mostly characterized by a smooth shape not containing any prominent point-like scatterers. Therefore, distributed scatterers are dominating so that the SBAS algorithm is the better choice.

4 Data Processing

For the Svartevann dam a larger number of ERS1/2 scenes have been acquired from ESA via a Category-I proposal. A total of 135 scenes could be acquired for the period 1992-2000. Of these scenes, 76 are in descending mode and 59 in ascending mode. In the ascending mode scenes Svartevann dam is located near the eastern edge; in the descending mode scenes, it is located near the scene's centre.

Figure 4 shows the footprints of the two different sets of SAR scenes together with the location of Svartevann dam and its reservoir.

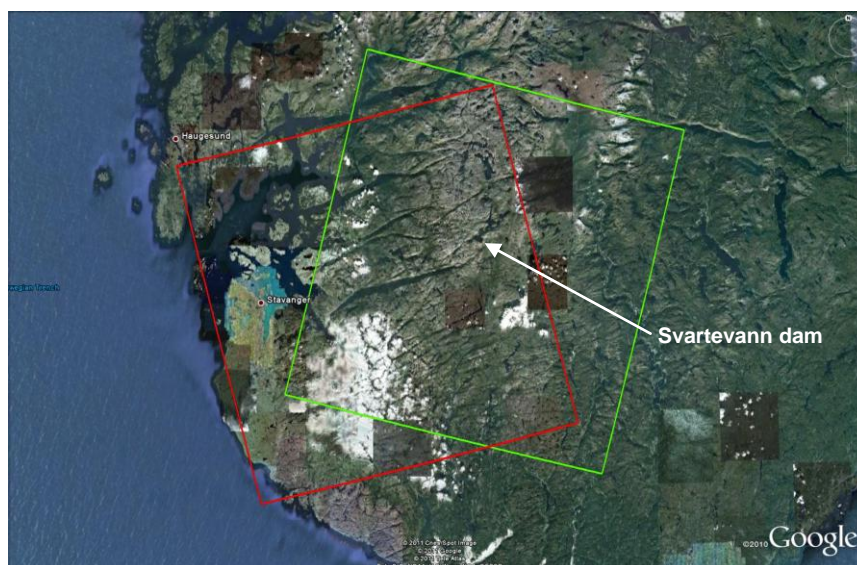


Figure 4: Footprints for ascending (red) and descending (green) ERS 1/2 scenes acquired for Svartevann dam

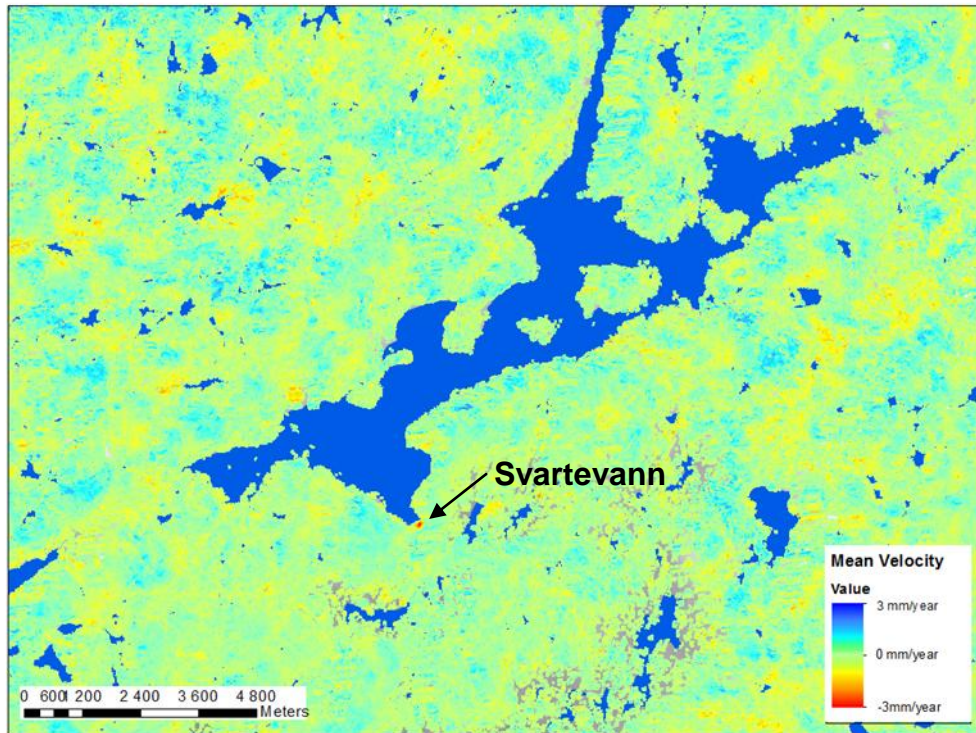


Figure 5: Color-coded ground velocity around the Svartevann reservoir in line of sight (23° incident angle) as derived from 23 ERS SAR scenes in ascending mode between 1992 and 2000

4.1 Ascending Mode Results

The image in Figure 5 shows displacements in the area around the reservoir derived from 23 ascending mode scenes using the SBAS algorithm. Since snow cover causes decorrelation of the interferometric phase the winter season scenes have been excluded from this subset. The yellow and turquoise colors indicate the absence of statistically relevant displacements around the reservoir. Only the dam it-self, marked with an arrow, shows a clear subsidence signal indicated by red colors. Figure 6 shows the ground velocity overlaid on an aerial photograph of Svartevann dam. Due to the high resolution of the satellite the detailed distribution pattern of the displacements over the dam can be seen. Compared to the geodetic displacement measurements carried out 4 years after completion of the dam (see Figure 3), the estimated ground velocities show the same overall pattern of a symmetric displacement at the centre of the dam crown. The maximum displacement velocity can be observed near the center of the crest with a value of approximately 3 mm/year. Because of the steep incidence angle of 23° , the LOS displacement can be best compared to the settlement map in Figure 3a. Naturally the displacement velocity between 1992 and 2000 is much lower compared to the one

measured just after completion of the dam (which was approx. 25cm/year), because the dam has had about 10 years more time to settle since then.

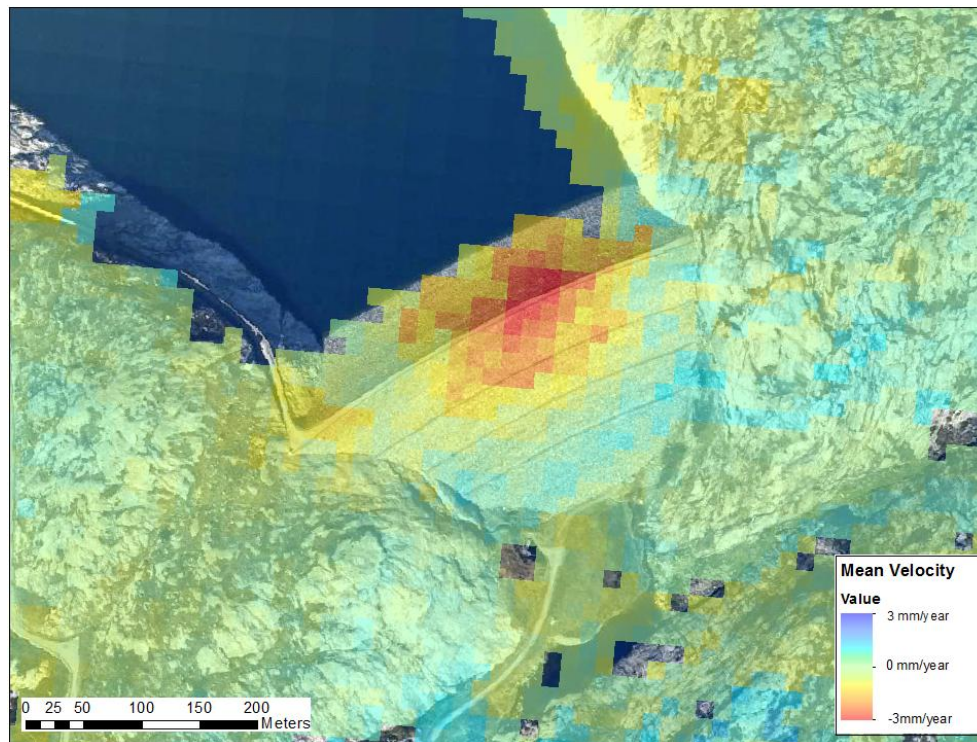


Figure 6: Same colour-coded ground velocities as in Figure 5 zoomed to the dam it-self. For an easier interpretation, the ground velocities are displayed on top of an aerial photograph of Svartevann dam.

An observation that can also be made in the results are pixels with estimated velocities that appear in the lake east of the dam. This is due to layover, an effect from the SAR acquisition geometry in combination with steep slopes. This results in multiple possible solutions for the range-Doppler equation. For layover areas, three (or more in extreme cases) pixels contribute, and since the water has a coherence of zero and the back-slope contribution usually is very weak, the foreslope contribution is often strong enough to preserve coherence. In the present version of the processing software, however, the geocoding always converges to the near range solution, which in this case is in the water. A newer implementation is under development which is masking layover areas already in the pixel selection step in order to avoid such kind of misplaced pixels.

As described in Section 3 the SBAS algorithm does not only provide the mean ground velocity over the observed time period, but gives us the complete time-series of displacement for each resolution cell. Figure 7 shows the displacement time-series for 5 positions evenly distributed along the crest of the dam. The time-series are somewhat

noisy, since only 18 SAR scenes passed the interferogram quality check and, thus, some atmospheric therefore effects might still be part of the displacement signal. Some time-series might also be affected by unwrapping errors, especially across the larger data gap between 1994 and 1995. The time-series at positions P2, P3 and P4 show that the subsidence near the center of the crest is getting weaker between 1995 and 2000, which is consistent with the observation above that the mean ground velocity between 1992 and 2000 is much less compared to the ground velocity between 1976 and 1980.

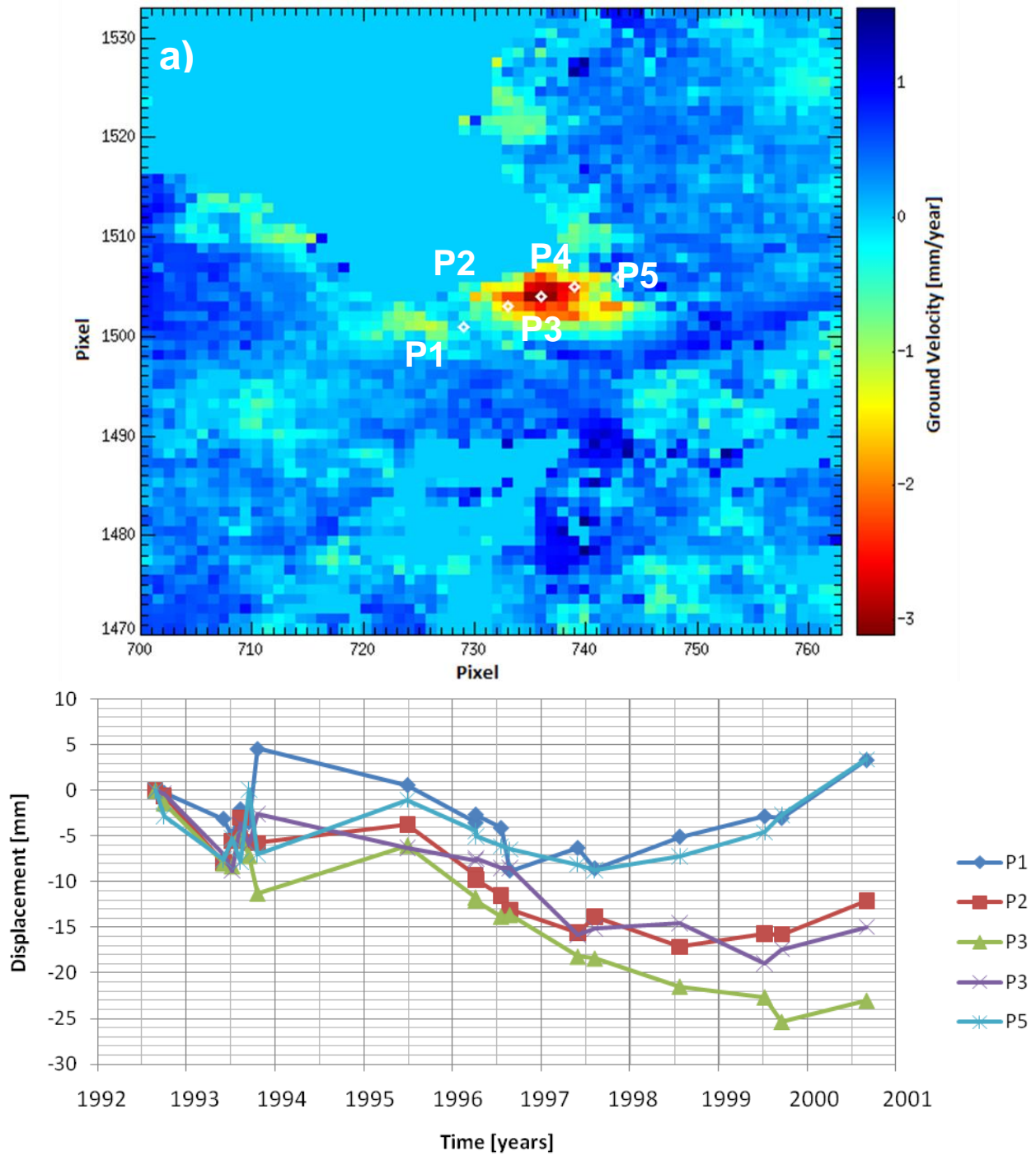


Figure 7: a) Mean ground velocity in radar geometry (not geocoded) with 5 positions marked along the crest of the dam; b) Displacement (in line of sight) time series for the positions marked in a). Negative displacement corresponds to a movement away from the satellite.

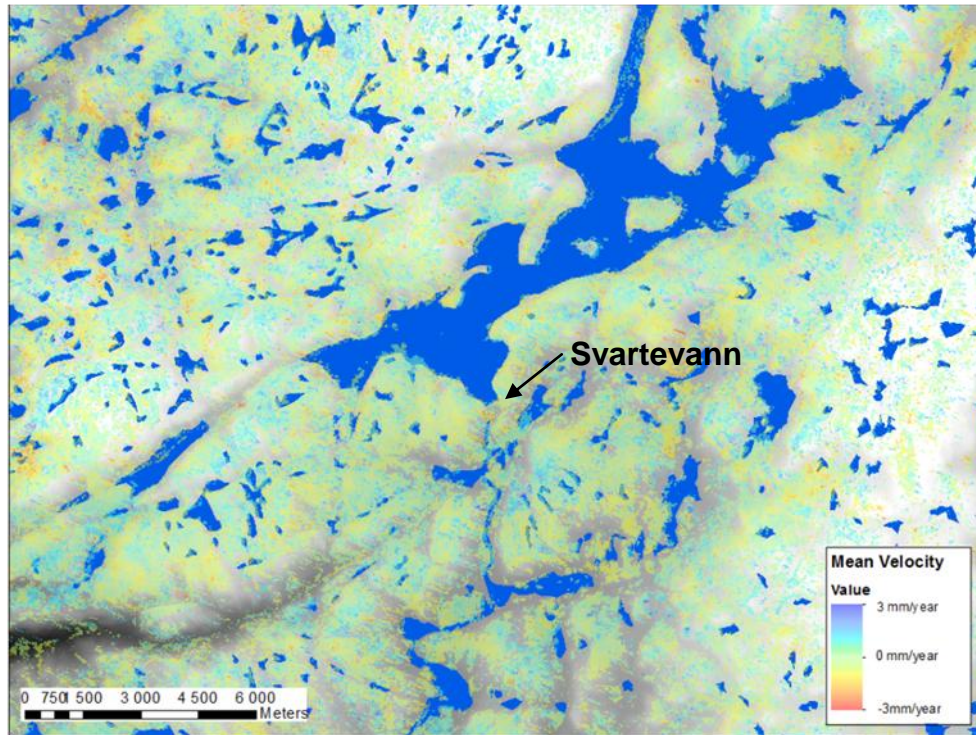


Figure 8: Color-coded ground velocity around the Svartevann reservoir in line of sight (23° incident angle) as derived from 22 ERS SAR scenes in descending mode between 1992 and 2000.

4.2 Descending Mode Results

The combined analysis of ascending and descending mode can give additional information about the direction of the movement because the orientation of the satellite and therefore the look angle of the radar beam is different in the respective acquisitions. While ascending mode scenes are acquired with a look direction approximately towards the east / southeast, the look direction of descending mode scenes is approximately west / northwest.

Figure 8 shows the mean ground velocity in line-of-sight for 22 descending mode scenes. Only 13 unique scenes passed the interferogram quality check, which is at the lower limit to allow for effective compensation of atmospheric effects. Figure 8 shows the ground velocity for the area surrounding the reservoir. Again we see large areas that are covered with estimated ground velocity values. This indicates an overall good coherence between the SAR scenes, although slightly weaker as compared to the results from the ascending mode scenes. The close-up image in Figure 9, however, reveals that the crest and the downstream slope of the dam are only covered by a limited number of estimated

velocities. Generally, a slightly weaker coherence can be observed. One reason for this might be that the quality of the SAR data is not as good as for the ascending mode scenes. Another reason can be an unfortunate constellation of the scenes, e.g., larger baselines or an uneven distribution of the scenes in time. The fact that the dam itself shows a particularly low coherence might also be due to a foreshortening effect. Foreshortening is a weaker form of the layover effect described above, where the range-Doppler equation still has a unique solution, however, the steep downstream slope of the dam still causes an across-track compression of the backscatter. During the SBAS processing line this is compensated using terrain information from a digital elevation model, however, the steeper the slope, the more error prone is the compensation.

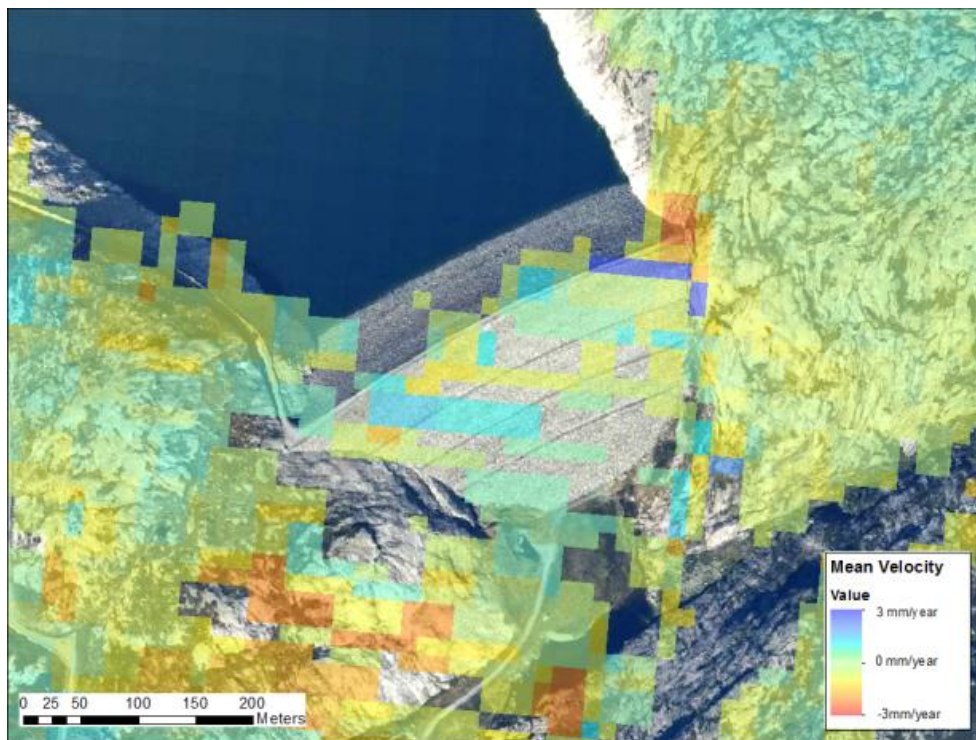


Figure 9: Same color-coded ground velocities as in Figure 8 zoomed the dam it-self. For an easier interpretation, the ground velocities are displayed on top of an aerial photograph of Svartevann dam.

5 Conclusions

The presented results show that SAR interferometry allows mapping of very local displacements at the dam as well as displacements on a regional scale around the reservoir. Due to the usually steep terrain in the area around dams and the steep slope of the dam it-self, the quality of the results strongly depend on the acquisition geometry. Also

the temporal sampling plays a very important role, and a minimum of 15 scenes is needed to achieve reliable results.

Despite these requirements, the method has a great potential for cost-efficient long-term monitoring. Compared to the ERS1/2 satellites used for this study today's and future satellites can provide much better data quality in terms of resolution, acquisition frequency and orbit accuracy. New satellites like Sentinel-1, TerraSAR-X or COSMO-SkyMed provide the possibility to acquire data stacks that are large enough for the SBAS processing chain within only two years. However, it has to be noted that data stacks from only one season will generally be too short since they contain large seasonal effects that cannot be modelled and thus not compensated.

With frame sizes – here exemplary for Radarsat-2 – in the range of 20x20km (ultra fine mode) to 150x150km (wide swath) the method even allows mapping displacements at multiple dams using the same set of SAR scenes, which makes it even more cost efficient.

6 Acknowledgements

The Research Council of Norway and the Norwegian Space Center provided financial funding for the presented work. Satellite data was provided by the European Space Agency under the Category-1 proposal 7678.

References

B. Kjærnsli, G. Kvale, J. Lunde, and J. Baade-Mathiesen, 1982. Design, Construction Control, and Performance of the Svartevann Earth-Rockfill Dam, NGI publication Nr. 142, 1982.

E. DiBiagio, F. Myrvoll, T. Valstad, 1982. Field Instrumentation, Observations, and Performance Evaluation of the Svartevann Dam, NGI publication Nr. 142, 1982.

D. Massonnet and K. L. Feigl, 1998. Radar Interferometry and its Application to Changes in the Earth's Surface. *Reviews of Geophysics*, 36, 4, 441-500.

A. Ferretti, C. Prati, and F. Rocca, 2000. Non-linear subsidence rate estimation using permanent scatterers in Differential SAR Interferometry. *IEEE Trans. Geosci. Remote Sens.*, 38(5): 2202-2212.

P. Berardino, G. Fornaro, R. Lanari, and E. Sansosti (2002). A New Algorithm For Surface Deformation Monitoring Based On Small Baseline Differential SAR Interferograms, IEEE Trans. Geosci. Remote Sens., 40, 2375–2383.

Authors

Dr. Malte Vöge

malte.voege@ngi.no

Dr. Yngvar Larsen

yngvar.larsen@norut.no

Dr. Regula Frauenfelder

regula.frauenfelder@ngi.no

NGI

Norwegian Geotechnical Institute

Sognsveien 72, 0855 Oslo, Norway

www.ngi.no/en

Norut

Northern Research Institute

Forskningsparken i Breivika, 9294 Tromsø

www.norut.no/tromso_en/